Received: Added at production | Revised: Added at production | Accepted: Added at production

RESEARCH ARTICLE

From Snapshots to Structure: A Novel Method for Reconstructing Directed Microbial Interaction Networks from Compositional Data

Ranjith N

[1] Independent Researcher, Chennai, Tamilnadu, India

Correspondence
Corresponding author Ranjith N,.
Email: ranjithn2012@gmail.com

Abstract

Microbial communities are shaped by complex ecological interactions that govern their structure, stability, and function. However, inferring these interactions from 16S rRNA gene sequencing data remains challenging due to data compositionality, limited temporal resolution, and the inability of traditional correlation-based methods to capture directionality or mechanistic influence. Microbial communities dynamically restructure in response to environmental and internal pressures, yet the ecological mechanisms guiding these transitions remain elusive. Here, we present a novel network inference framework that reconstructs directed, signed, and weighted microbial interaction networks from cross-sectional compositional data, without relying on predefined dynamic models or time-series sampling. By estimating asymmetric slopes and applying a perturbation-informed inference strategy, the method infers ecological interaction polarity and strength while accounting for compositional constraints. Applied to a synthetic gut microbiome dataset, the framework revealed taxon-specific trajectories, directional ecological dependencies, and hierarchically organized interaction networks. Persistent Directed Acyclic Graph (DAG) motifs identified keystone initiators, while other taxa emerged as resilient, high-connectivity hubs. A quadrant-based network visualization was introduced to enhance interpretability by distinguishing ecological influencers from responders based on interaction flow. The inferred networks demonstrated strong alignment between interaction polarity and abundance trends, revealing a robust ecological principle polarity-driven succession whereby the net balance of cooperative and antagonistic interactions predicts species abundance trajectories and community dynamics. This mechanistic insight advances microbial ecology by enabling predictive interpretations from cross-sectional datasets and broadening the theoretical understanding of microbial interaction networks. The approach supports scalable, hypothesis-driven analysis of microbial communities across environments and holds particular promise for guiding microbiome engineering, synthetic consortia design, and the retrospective analysis of public microbiome repositories.

KEYWORDS
Microbiome, Ecological Interactions, 16S Amplicon Metagenomics, Directed Networks, Cartesian plot.

1 | INTRODUCTION

Microbial communities dynamically restructure in response to both environmental and internal pressures, yet the ecological mechanisms governing these transitions remain poorly understood. This work introduces a novel network inference framework capable of extracting directional, signed, and weighted interactions among microbial taxa from compositional (16S) data. Application of the method reveals a robust ecological principle, termed polarity-driven succession, in which the net balance of cooperative and antagonistic interactions predicts species abundance trajectories and overall community dynamics. This mechanistic insight advances microbial ecology by enabling predictive interpretations from static, cross-sectional datasets and broadening the theoretical understanding of microbial interaction networks. The results also support the hypothesis that pairwise linear associative interactions, when organized into a directed acyclic graph (DAG), can approximate nonlinear abundance dynamics via cumulative net effects propagated through the network. In this context Network-based frameworks have emerged

Abbreviations: DAGs, Directed Acyclic Graphs; CLR, Centred Log-ratio Normalization .

as powerful tools for representing and analyzing microbial interactions, thus providing a conceptual toolkit to link topological features of a given interaction network to its ability to perform functions[1]. In these ecological networks, nodes represent microbial taxa and edges represent direct ecological abundance driven interactions such as mutualism, parasitism, commensalism, amensalism, or competition. Directed, signed, and weighted ecological networks have the potential to capture the causality and intensity of these interactions, offering a mechanistically grounded view of community dynamics. However, most microbial networks constructed from 16S rRNA gene amplicon sequencing data rely on correlation or co-occurrence measures, which produce undirected associations that do not reflect causal or mechanistic relationships[2]. These approaches also tend to produce visually complex graphs, often referred to as the hairballs, which obscure interpretability and hinder practical application[3,4]. A further complication arises from the compositional nature of 16S sequencing data, which report relative rather than absolute taxon abundances. This constraint introduces statistical artifacts unless compositionality is properly accounted for[5]. Methods such as SparCC and SPIEC-EASI address this by applying log-ratio transformations, notably the centered log-ratio (CLR), to estimate sparse correlation or precision matrices[6]. Nonetheless, these methods yield undirected networks and do not infer the direction, sign, or magnitude of ecological effects, limiting their ecological interpretability. Causal inference methods using time-series or multi-omic data have been developed to overcome these limitations. These approaches can, in principle, infer directionality and functional relationships but generally require dense longitudinal sampling or rich metadata, which are rarely available in most microbiome studies. Moreover, time-series based inference methods suffer from two major limitations. First, they typically rely on the selection of parameterized population dynamics models, which is challenging given the diversity of microbial interactions and nonlinear behaviors that can arise even in small systems[7]. Second, informative time-series data are difficult to obtain in many microbial systems, particularly host-associated communities such as the human gut microbiota, which often exhibit stability and resilience. As a result, available data largely reflect steady-state behavior, limiting the informativeness of dynamic models. Invasive perturbations aimed at increasing temporal variation may be impractical or ethically untenable in human or animal studies. To address these challenges, this study presents a nove mathematical inference framework that infers directed, signed, and weighted ecological interactions directly from cross-sectional 16S rRNA data. This method estimates asymmetric slopes between microbial taxa to approximate interaction directionality and employs adaptive perturbation analysis to assess effect sign and strength. By correcting for compositionality and avoiding reliance on predefined dynamic models or time-resolved data, this approach enables the inference of biologically interpretable networks from widely available steady-state datasets. A biologically optimized visualization strategy is also proposed to enhance interpretability and minimize visual clutter of hairballs, facilitating insight into microbial community structure and dynamics, Along with this Consistent DAGs (Directed Acyclic Graphs) across conditions are identified and analyzed for downstream interpretation. The growing availability of metagenomic and multi-omic datasets, including many generated for unrelated experimental objectives, presents a major opportunity for large-scale ecological analysis. When systematically reused in conjunction with robust inference frameworks such as the one proposed in this study, these datasets can significantly advance the understanding of intermicrobial interactions, support hypothesis generation, and guide targeted experimental validation[8].

2 | METHODOLOGY

2.1 | Data Acquisition and Pre-processing

We used publicly available OTU count data from the study “Inter-species Metabolic Interactions in an In-vitro Minimal Human Gut Microbiome of Core Bacteria”, which includes time-series 16S rRNA amplicon sequencing of a defined in-vitro microbial consortium[9]. The dataset comprises 20 samples: four biological replicates (B1–B4) sampled at five time points (T0, T24, T48, T72, and T96 hours). The microbial community is composed of ten well-characterized human gut bacterial species, making it an ideal model for inter-species ecological interaction analysis. Raw OTU tables were downloaded from the study’s GitHub repository. No additional taxonomic classification or metagenomic processing was performed, as the species-level OTUs were pre-defined.

TABLE 1 Abundances of microbial taxa across replicates.

Taxon	B1T0	B2T0	B3T0	B4T0	B1T24	B2T24	B3T24	B4T24	B1T48	B2T48	B3T48	B4T48	B1T72	B2T72	B3T72	B4T72	B1T96	B2T96	B3T96	B4T96
Agathobacter rectalis	904	607	599	1253	1982	339	5418	10386	2875	1452	2650	4340	1920	2498	1345	1181	2320	2033	10838	8122
Anaerobutyricum soehngenii	302	233	266	173	14	3	30	267	23	21	45	9	13	21	8	16	14	18	54	48
Bacteroides ovatus	599	325	326	797	1238	267	2391	1343	2475	934	1730	993	1169	1122	663	220	820	1292	3830	1014
Bacteroides xylanisolvens	1125	605	750	1536	2482	559	4836	2395	5046	1858	3401	1766	2367	2056	1249	362	1682	2672	7297	1882
Coprococcus catus	223	149	158	224	301	61	119	231	206	128	57	19	84	127	43	3	103	121	209	52
Eubacterium siraeum	6661	4948	5706	7594	11841	2238	10962	3047	13847	7580	5108	3172	8790	10657	2489	2540	8463	7439	12889	13416
Faecalibacterium prausnitzii	3479	2582	2923	4092	5859	1183	5688	1922	6535	3759	2959	1831	4399	4930	1401	1331	4220	4156	8450	7552
Lachnospiraceae bacterium	692	452	462	512	598	115	790	1150	1110	610	600	617	726	789	404	252	1068	892	3530	2371
Roseburia intestinalis	573	388	469	1947	3872	569	619	2316	616	168	53	32	127	97	24	7	77	71	90	42
Subdoligranulum variabile	118	105	105	71	24	3	108	196	28	22	157	138	22	38	93	64	46	37	655	554

Source: Data from "Inter-species Metabolic Interactions in an In-vitro Minimal Human Gut Microbiome of Core Bacteria" (Shetty et al., 2022), Available at https://github.com/microsud/Db-MM-10/blob/master/data/03_amplicon/tables/otu_table.csv .

2.2 | Compositional Data Normalization

To address the compositional nature of microbial abundance data, centered log-ratio (CLR) transformation was applied[5]. For each sample, CLR normalization was computed across all ten species, resulting in a transformed abundance matrix suitable for downstream correlation and regression analyses.

TABLE 2 CLR-normalized abundances of microbial taxa across replicates.

Name	B1T0	B2T0	B3T0	B4T0	B1T24	B2T24	B3T24	B4T24	B1T48	B2T48	B3T48	B4T48	B1T72	B2T72	B3T72	B4T72	B1T96	B2T96	B3T96	B4T96
Agathobacter rectalis	0.21	0.19	0.09	0.43	0.92	0.83	1.72	2.16	1.18	1.15	1.55	2.55	1.42	1.52	1.66	2.18	1.58	1.39	1.95	2.25
Anaerobutyricum soehngenii	-0.89	-0.76	-0.72	-1.55	-4.04	-3.89	-3.48	-1.50	-3.65	-3.09	-2.52	-3.63	-3.57	-3.26	-3.47	-2.12	-3.53	-3.34	-3.35	-2.88
Bacteroides ovatus	-0.20	-0.43	-0.51	-0.02	0.44	0.59	0.90	0.11	1.03	0.71	1.13	1.07	0.93	0.72	0.95	0.50	0.54	0.94	0.91	0.17
Bacteroides xylanisolvens	0.43	0.19	0.32	0.63	1.14	1.33	1.61	0.69	1.74	1.39	1.80	1.65	1.63	1.33	1.59	1.00	1.26	1.66	1.55	0.79
Coprococcus catus	-1.19	-1.21	-1.24	-1.29	-0.97	-0.88	-2.10	-1.65	-1.46	-1.28	-2.28	-2.88	-1.71	-1.46	-1.78	-3.79	-1.53	-1.43	-2.00	-2.80
Eubacterium siraeum	2.21	2.29	2.35	2.23	2.70	2.72	2.43	0.93	2.75	2.80	2.21	2.23	2.94	2.97	2.27	2.95	2.87	2.69	2.12	2.75
Faecalibacterium prausnitzii	1.56	1.64	1.68	1.61	2.00	2.08	1.77	0.47	2.00	2.10	1.67	1.68	2.25	2.20	1.70	2.30	2.18	2.11	1.70	2.17
Lachnospiraceae bacterium	-0.06	-0.10	-0.17	-0.47	-0.28	-0.25	-0.21	-0.04	0.23	0.28	0.07	0.60	0.45	0.37	0.46	0.64	0.80	0.57	0.83	1.02
Roseburia intestinalis	-0.25	-0.25	-0.15	0.87	1.59	1.35	-0.45	0.66	-0.36	-1.01	-2.36	-2.36	-1.29	-1.73	-2.37	-2.94	-1.83	-1.96	-2.84	-3.02
Subdoligranulum variabile	-1.83	-1.56	-1.65	-2.44	-3.50	-3.89	-2.20	-1.81	-3.45	-3.04	-1.27	-0.90	-3.05	-2.66	-1.01	-0.73	-2.34	-2.62	-0.86	-0.44

[a]CLR: Centered log-ratio transformation.
Source: Data generated from compositional transformation of microbial abundances.

TABLE 3 Mean CLR-normalized abundances of microbial taxa across replicates.

Taxon	T0	T24	T48	T72	T96
Agathobacter rectalis	0.23172264598	1.40640406615	1.60673929504	1.69658282278	1.79136563858
Anaerobutyricum soehngenii	-0.97969293658	-3.22795648659	-3.22289719845	-3.10343972843	-3.27616476084
Bacteroides ovatus	-0.29254656998	0.51317191773	0.98364673755	0.77547840281	0.63781402565
Bacteroides xylanisolvens	0.39268794310	1.19250238895	1.64660292505	1.38609449630	1.31483927269
Coprococcus catus	-1.23291648956	-1.39960406804	-1.97702395871	-2.18511117079	-1.94254392099
Eubacterium siraeum	2.26953144699	2.19470561327	2.49857016141	2.78490922811	2.60800258461
Faecalibacterium prausnitzii	1.62273737955	1.58020925996	1.86164188804	2.11389829507	2.03927874977
Lachnospiraceae bacterium	-0.19746686724	-0.19496713889	0.29297010401	0.47847483208	0.80321404994
Roseburia intestinalis	0.05487842741	0.78579184730	-1.52306343882	-2.08309973212	-2.41257715021
Subdoligranulum variabile	-1.86893497968	-2.85025739983	-2.16718651513	-1.86378744581	-1.56322848920

[a]Values represent average CLR-transformed abundance across samples.
Source: Data generated from averaging the replicates of CLR-transformed abundance across samples.

2.3 | Correlation Analysis and Filtering

To identify potential microbial associations, co-occurrence-based correlation analysis was performed, considering only the subset of samples where both species in a given pair were present (non-zero abundance) within the replicates. This avoids

the confounding effects of sparsity and zero-inflation common in microbiome datasets. For each condition with replicates, all possible permutations of species pairs were considered. For each pair, correlation was computed using only the replicate samples in which both species had non-zero CLR-normalized abundances [10]. Pairs with fewer than three such co-occurrence points ($n < 3$) should be excluded. For the remaining pairs, both Pearson and Spearman correlation coefficients were calculated. A pair was retained if at least one of the two correlation types was statistically significant ($p < 0.05$). This procedure yielded a reduced set of high-confidence co-occurring species pairs for each condition, used in downstream inference [10].

2.4 | Linear Regression Slope based Directionality Inference

To infer the direction of influence between significantly co-occurring species pairs, A slope asymmetry-based approach was employed. For each pair, two separate linear regressions were fitted: one predicting species Y from species X, and another predicting X from Y. The slopes from both models were then compared. Directionality was assigned based on a threshold criterion: if the absolute slope in one direction was at least 1.5 times larger than in the reverse direction, the pair was assigned a direction (e.g., X → Y). If neither direction clearly dominated, the pair was considered undirected and removed. This method captures underlying ecological asymmetries and is suitable for inferring causal tendencies in cross-sectional or replicate-based data. Inspired by Blöbaum et al(2019)'s method of inferring causal direction by comparing regression errors (MSE) [11], a simplified slope-asymmetry based heuristic framework was applied here, which is computationally lighter and well-suited to low-replicate ecological data was proposed.

Two paired samples of real numbers were used, where each set representing speceis's CLR abundance within a condition:

$$x = (x_1, x_2, \ldots, x_n), \quad y = (y_1, y_2, \ldots, y_n)$$

with $n \geq 3$ and non zero pairs data ≥ 3.

2.4.1 | Calculate basic statistics

$$n = |x| = |y|$$

$$S_x = \sum_{i=1}^{n} x_i, \quad S_y = \sum_{i=1}^{n} y_i$$

$$S_{xy} = \sum_{i=1}^{n} x_i y_i, \quad S_{x^2} = \sum_{i=1}^{n} x_i^2, \quad S_{y^2} = \sum_{i=1}^{n} y_i^2$$

2.4.2 | Calculate covariance and variances

$$\mathrm{Cov}(x, y) = \frac{1}{n} S_{xy} - \left(\frac{S_x}{n}\right)\left(\frac{S_y}{n}\right)$$

$$\mathrm{Var}(x) = \frac{1}{n} S_{x^2} - \left(\frac{S_x}{n}\right)^2, \quad \mathrm{Var}(y) = \frac{1}{n} S_{y^2} - \left(\frac{S_y}{n}\right)^2$$

2.4.3 | Calculate slopes

$$m_{y|x} = \frac{\mathrm{Cov}(x, y)}{\max(\mathrm{Var}(x), \varepsilon)}, \quad m_{x|y} = \frac{\mathrm{Cov}(x, y)}{\max(\mathrm{Var}(y), \varepsilon)}$$

with small $\varepsilon > 0$ to avoid division by zero.

2.4.4 | Determine dominant direction

With threshold $T = 1.5$,

$$\text{if } |m_{y|x}| > T \cdot |m_{x|y}| \implies D = '>' \quad (x \to y)$$

$$\text{else if } |m_{x|y}| > T \cdot |m_{y|x}| \implies D = '<' \quad (y \to x)$$

$$\text{otherwise } D = '?'$$

2.5 | Local Perturbation Analysis for Effect Direction

To characterize the type of interaction (e.g., Mutualism or Competition), local perturbation analysis on the CLR-normalized abundance data was performed. For each directed pair, a small positive and negative changes was simulated in the source species's abundance and used the regression slope to estimate the resulting change in the target species. The consistency and direction of these changes determined the interaction types as in mutualism (++), competition (−−), parasitism/predation (`+- and -+`) and Undefined (?): inconsistent or unclear directional effects. This analysis allows the classification of pairwise microbial interactions without requiring mechanistic models or dynamic simulations.

2.5.1 | Perturbation analysis

$$\text{perturb} = \begin{cases} x & D = '>' \\ y & D = '<' \end{cases}, \quad \text{observe} = \begin{cases} y & D = '>' \\ x & D = '<' \end{cases}$$

For each $i = 1, \ldots, n$:

- Ignore if $|\text{perturb}_i| < \delta_0$ or $|\text{observe}_i| < \delta_0$ ($\delta_0 \approx 10^{-10}$).
- Adaptive perturbation:

$$\Delta_i = \max(0.1 \times |\text{perturb}_i|, 0.01)$$

- Positive perturbation:

$$p_i^+ = \text{perturb}_i(1 + \Delta_i)$$
$$d_i^+ = m(p_i^+ - \text{perturb}_i)$$

- Negative perturbation:

$$p_i^- = \text{perturb}_i(1 - \Delta_i)$$
$$d_i^- = m(p_i^- - \text{perturb}_i)$$

2.5.2 | Match signs

Let $s = \text{sign}(m)$.
Count:

$$C^+ = \#\{i : \text{sign}(d_i^+) = s\}, \quad C^- = \#\{i : \text{sign}(d_i^-) = s\}$$

Track effect sign frequencies for d_i^+ and d_i^-.

2.5.3 | Dominant perturbation

If $C^+ \geq C^-$, dominant perturbation sign = '+', else '-'.

2.5.4 | Final notation

$$\text{vardirect} = \text{dominant perturbation sign/most frequent effect sign}$$

2.5.5 | Relative effect strength

$$r = \begin{cases} \frac{|m_{\text{ylx}}|}{\max(|m_{\text{xly}}|, \varepsilon)} & D = '>' \\ \frac{|m_{\text{xly}}|}{\max(|m_{\text{ylx}}|, \varepsilon)} & D = '<' \end{cases}$$

2.5.6 | Output

$$(D, r, \text{vardirect}, |m|)$$
$$D = Direction(<, >),$$
$$r = Rateofeffect,$$
$$vardirect = Interactionsign(+/+, +/-, -/+, --),$$
$$m = Slopemagnitude,$$

2.6 | Network Construction and Visualization

To enhance the interpretability of microbial interaction networks, a novel visualization framework based on a Cartesian grid system was developed[2]. In this approach, species were placed along the x and y axes according to their degree centrality within the network, replacing traditional numeric units with species names. Ecological interactions were then plotted as directional edges within the appropriate quadrants of the grid, corresponding to their qualitative effects: mutualism (++), competition (−−), parasitism/predation (+- and −+)[12,2,1]. The magnitude of each interaction was represented by the size of slope-indicative bubbles. This design avoids node overlap and visual clutter commonly encountered in traditional network diagrams, providing a clearer representation of directional influence and interaction strength in simplified synthetic microbiome systems.

2.7 | Cross-Condition DAG Construction and Comparison

Directed acyclic graphs (DAGs) are a well-established framework in causal inference, forming a foundational component of path analysis and structural equation modeling. While DAGs are widely used in fields such as statistics and epidemiology, their application remains relatively limited in the biological sciences, particularly in microbial ecology[13]. In this study, DAGs were used to represent directional dependencies and non-linear interactions within microbial taxa across multiple experimental conditions. To identify consistent interactions, DAGs inferred from each condition-specific dataset were aggregated and compared. Recurrent subgraphs particularly stable three node motifs were identified by aligning DAG structures across conditions. These were subsequently visualised to highlight interaction patterns that persist regardless of environmental variation or temporal stratification.

3 | RESULTS

CLR-normalized barplots illustrated temporally resolved microbial abundance dynamics, revealing distinct compositional shifts across the experimental timepoints. Several taxa, including *Agathobacter rectalis*, *Bacteroides xylanisolvens*, *Bacteroides ovatus*, and *Lachnospiraceae bacterium*, exhibited a consistent increase in CLR values, suggesting successful adaptation and a potential ecological advantage under the imposed conditions. Conversely, *Anaerobutyricum soehngenii*, *Roseburia intestinalis*, and *Coprococcus catus* showed marked declines, indicative of environmental sensitivity or suppression by competitive interactions. *Eubacterium siraeum* and *Faecalibacterium prausnitzii* maintained stable, high CLR values, positioning them as resilient core members of the microbiota.

To probe interspecies ecological dependencies, all 45 possible pairwise interactions among the 10 dominant taxa were assessed across five timepoints (T0, T24, T48, T72, T96) using permutation-based association testing where the novel framework was applied to infere the interactions. On average, 37 interactions per timepoint were seen, with interaction counts of 40, 36, 37, 37, and 36 were shortlisted respectively. Eco-Cartesian plots of these interactions highlighted structured, directional associations that evolved over time, capturing the abundance based dependence. Higher-order microbial interactions were further examined through Directed Acyclic Graphs (DAGs), capturing conditional dependencies among taxa, though multiple DAGs were found only 9 were represented here which has species > 2 and spanning timepoints > 2. Among the nine DAGs, five persisted consistently from T48 to T96. These persistent interaction motifs were all initiated by *Lachnospiraceae bacterium*, suggesting its potential role as a keystone or ecological initiator. Intermediate nodes within these motifs frequently included *Agathobacter rectalis*, *Anaerobutyricum soehngenii*, *Roseburia intestinalis*, and *Eubacterium siraeum*, while *Subdoligranulum variabile* was often observed as a terminal responder, reflecting its downstream positioning in the network.

The reconstructed interaction network demonstrated a non-random, hierarchically organized topology, where species ranked by degree centrality positioned highly connected taxa centrally and less connected ones peripherally across all axes. This spatial arrangement enabled clear visualization of interaction cascades: positive and negative symmetric interactions (+/+, -/-) clustered in quadrants I and III, while asymmetric polarity cascades (+/-, -/+) appeared in quadrants II and IV, facilitating comprehensive assessment of interaction dynamics across the network. Temporal shifts in incoming interaction strength closely mirrored species abundance trajectories consistently across replicates which can be seen in CLR barplots, further corroborated by quadrant-specific network analyses. Together, these results reveal an emergent ecological principle in which microbial

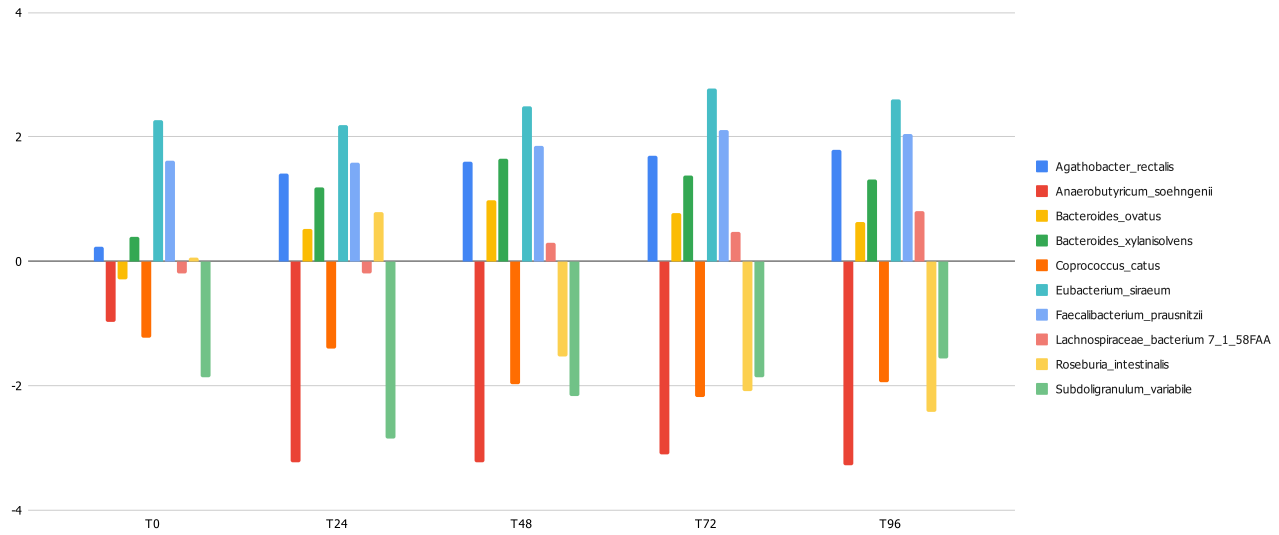

FIGURE 1 CLR-normalized mean barplot of microbial taxa across replicates.

community restructuring is governed by the balance of positive and negative interactions, with dominant taxa possessing more supportive positive links with magnitude over negative links, while suppressed species endure greater antagonistic pressures. This polarity-based framework offers a unified explanation for abundance shifts and directional changes in microbial community architecture during ecological succession.

4 | DISCUSSION

Understanding the ecological interactions that underpin microbial community structure is central to deciphering their functional dynamics and stability. Microbial ecosystems exhibit a wide range of interspecies relationships, from mutualism and syntrophy to competition and antagonism, which collectively shape their composition and resilience. However, inferring these interactions remains challenging due to the compositional nature of sequencing data, high dimensionality, and inherent sparsity in microbiome datasets. Traditional approaches, such as taxonomic bar plots or correlation-based networks, offer only coarse, descriptive insights and fail to capture directionality, causality, or mechanistic underpinnings of microbial interactions [14,4,15].

A major limitation of many existing methods is their dependence on undirected co-occurrence or correlation matrices, which are prone to conflating direct and indirect associations. Furthermore, such methods typically do not account for the statistical distortions introduced by the compositionality of relative abundance data, often leading to spurious inferences [5]. Although tools like SparCC and SPIEC-EASI address some of these constraints, they generally produce undirected graphs and are unable to infer interaction sign or strength, which limits their utility in modeling dynamic community behavior [16].

To overcome these barriers, a novel network inference framework was developed that reconstructs directed, signed, and weighted microbial interaction networks from cross-sectional compositional datasets [7]. Without relying on time-series data or predefined mechanistic models, this method leverages asymmetric slope estimation and dual-value perturbation heuristics to infer the directionality and polarity of interactions. The approach thus enables a shift from static, descriptive microbiome profiling to mechanistic ecological interpretation, allowing microbial taxa to be categorized based on their functional roles such as ecological influencers, responders, or structural hubs.

One of the key advantages of this approach is its capacity to identify critical taxa based on network topology. By employing degree centrality metrics, nodes with extensive connectivity and control over interaction flow are prioritized. In a microbiome context, such nodes may serve as ecological keystones or hubs, influencing the broader community through direct and indirect interactions [15,1].

A distinguishing feature of this work is the introduction of a customized visualization technique tailored for ecological networks. Unlike conventional network diagrams that often result in visually dense and uninterpretable hairballs due to undirected,

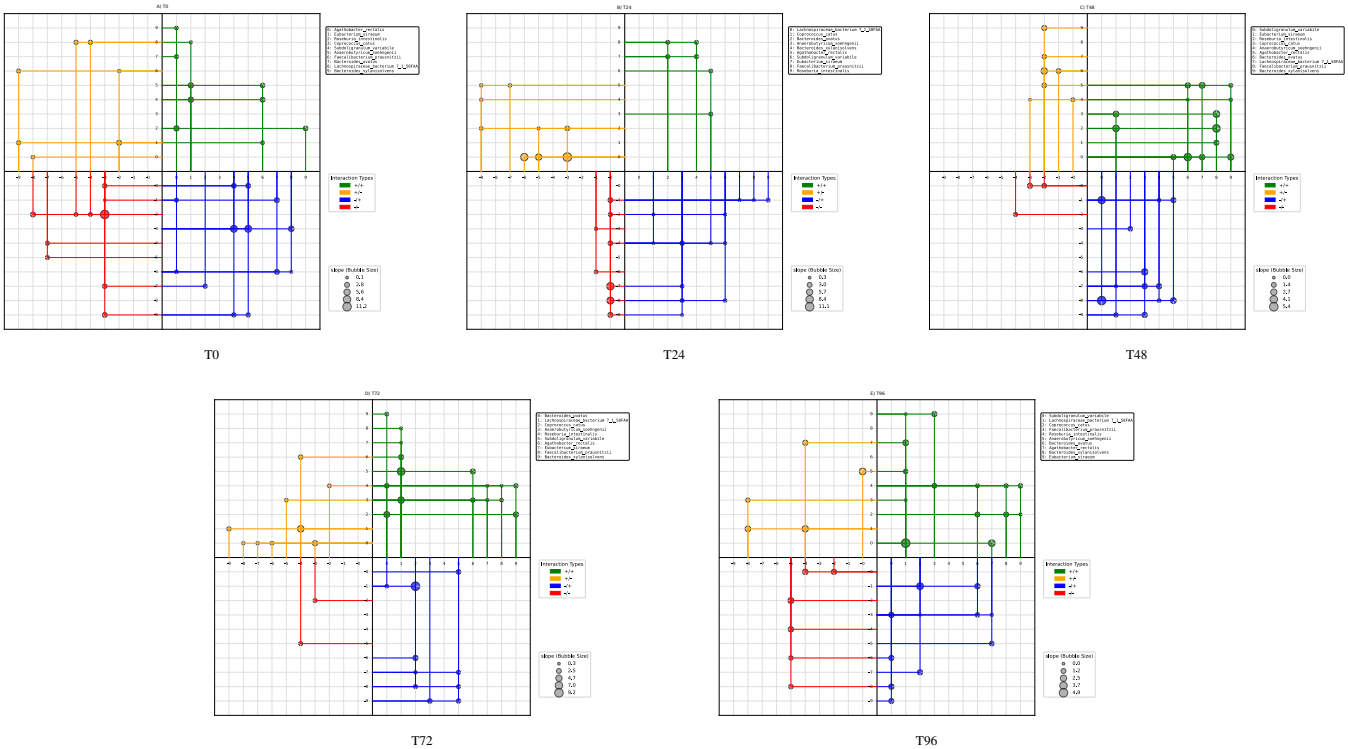

FIGURE 2 Directed, signed Eco-Cartesian interaction network inferred from centered log-ratio (CLR) normalized abundance data. Nodes placed on all the axis, that represent microbial species orderd by degree centrality, positioned according to a custom quadrant-based layout that separates outgoing (influencing) from one axis to incoming (receiving) interactions on next axis in counter-clockwise direction. Edge direction indicates the inferred ecological influence from one taxon to another; edge color denotes interaction type; and edge bubbles corresponds to interaction strength (slope magnitude). This layout facilitates intuitive interpretation of species-level roles, highlighting ecological influencers, responders, and taxa under net antagonistic or cooperative pressure. The visualization mitigates the hairball effect and allows direct comparison of network dynamics with abundance trends within a sample and across time points at T0, T24, T48, T72, and T96 hours.

overlapping edges[4], the proposed layout separates microbial abundance dependent interactions into directional quadrants that distinguish between outgoing and incoming interactions. This quadrant-based visualization enhances interpretability by directly linking topological attributes with ecological function. For instance, taxa with high incoming negative influence and magnitude often correspond with reduced relative abundance and viceversa, while those with strong outgoing positive influence and magnitude may drive community dynamics and viceversa as important ecological drivers. The design minimizes edge clutter and retains topological clarity even as network size increases, making it suitable for high-complexity datasets.

The inferred interaction networks also enable deeper ecological interpretation. Taxa with high cumulative outgoing influence can be viewed as potential keystone species[1], while others consistently positioned as recipients of negative interactions may represent suppressed or competitively disadvantaged members. Moreover, motif analysis within these networks reveals ecologically relevant structures such as cascades, control modules, and signal integration patterns providing mechanistic insights into community level functions[17].

Using a publicly available synthetic dataset, the framework was applied to identify key driver taxa, conditionally persistent DAG motifs, and temporal rewiring of microbial influence patterns. Although the dataset was not generated specifically for this method, the consistent emergence of interpretable ecological structures such as the initiator role of *Lachnospiraceae bacterium* supports the validity of the approach.

This network-based framework has practical implications for microbial cultivation and synthetic community design. By identifying potential mutualists or antagonists, it facilitates the strategic co-culturing of fastidious or previously uncultured microbes. Such insights are especially valuable in biotechnological and clinical contexts, where controlled manipulation of microbial communities is essential[18].

Additionally, the method is well-suited for integration with the rapidly expanding repository of publicly available microbiome datasets. Its reliance solely on cross-sectional relative abundance data allows retrospective application across thousands of studies. This opens pathways for resource efficient research, particularly in settings with limited access to experimental infrastructure, and promotes equitable participation in global microbiome science[8,19].

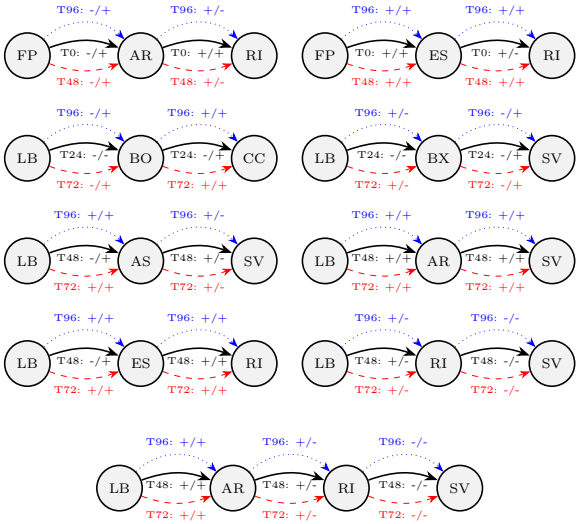

FIGURE 3 The Directed Acyclic Graphs (DAGs) illustrate the inferred directional interactions among microbial taxa that persist across multiple timepoints, revealing hierarchical ecological dependencies within the community. Each node represents a microbial species, and arrows indicate the direction of influence, capturing the potential flow of ecological impact from one taxon to another. These DAGs highlight conditionally persistent high-order interactions, emphasizing taxa that consistently act as initiators or responders over time. For clarity in visualization, each taxon is represented by a two-letter abbreviation: AR for *Agathobacter rectalis*, AS for *Anaerobutyricum soehngenii*, BO for *Bacteroides ovatus*, BX for *Bacteroides xylanisolvens*, CC for *Coprococcus catus*, ES for *Eubacterium siraeum*, FP for *Faecalibacterium prausnitzii*, LB for *Lachnospiraceae bacterium*, RI for *Roseburia intestinalis*, and SV for *Subdoligranulum variabile*.

When used in combination with advanced visualization tools such as Cytoscape and Hive plots, the interpretability and accessibility of these ecological networks are further enhanced[20]. As microbiome datasets continue to grow in scale and complexity, the need for methods that balance computational rigor with ecological relevance becomes increasingly important. The approach outlined here represents a scalable, data efficient, and mechanistically informative solution to microbial interaction inference, paving the way for more predictive and hypothesis driven microbiome research.

In summary, the developed network inference method provides a principled framework for mapping microbial ecological interactions from cross-sectional compositional data. It addresses key methodological challenges and enables a more nuanced understanding of microbial community structure, ecological roles, and potential functional dynamics[7].

5 | CONCLUSIONS

This study introduces a novel framework for inferring directed, signed, and weighted ecological interaction networks from cross-sectional, compositional 16S rRNA sequencing data. By addressing core limitations of traditional correlation-based approaches including lack of directionality, ecological polarity, and compositional bias this method enables a more mechanistically grounded interpretation of microbial community interactions. The framework operates under the assumption of quasi-steady-state conditions within individual timepoints, allowing for meaningful ecological inference in the absence of dense time-series data or predefined dynamic models. It leverages asymmetric slope estimation and adaptive perturbation heuristics to infer interaction direction, sign, and strength while accounting for the constraints of compositional data. Validation on a publicly available, temporally resolved synthetic dataset demonstrated the framework's capacity to recover consistent and ecologically plausible interaction patterns, including conditionally persistent network motifs and interpretable topological structures. These findings support the method's robustness and generalizability across datasets not originally designed for network inference. A biologically optimized quadrant-based visualization strategy further enhanced the interpretability of the resulting networks, facilitating the identification of functionally distinct ecological roles without introducing visual complexity typical of traditional network layouts. Overall, this approach provides a scalable, data-efficient, and biologically interpretable tool for microbial interaction inference. Its compatibility with widely available cross-sectional datasets offers new opportunities for predictive microbiome research, mechanistic hypothesis generation, and the design of targeted experimental or synthetic community interventions.

DATA AVAILABILITY

All the datasets anlalysed in this study are either publicly available or kindly provided by the original authors. Other data that supports the findings of this study are available from the correpoinding author on resonable requests.

ACKNOWLEDGMENTS

The author acknowledges the creators of the publicly available dataset from the study "Inter-species Metabolic Interactions in an In-vitro Minimal Human Gut Microbiome of Core Bacteria" (Shetty et al., 2022), whose valuable data made this analysis possible.

CONFLICT OF INTEREST

This research did not receive any funding. The author declares no conflict of interest.

REFERENCES

1. Oña L, Shreekar SK, Kost C. Disentangling microbial interaction networks. *Trends in Microbiology.* 2025.
2. Dohlman AB, Shen X. Mapping the microbial interactome: Statistical and experimental approaches for microbiome network inference. *Experimental Biology and Medicine.* 2019;244(6):445–458.
3. Jiang D, Armour CR, Hu C, et al. Microbiome multi-omics network analysis: statistical considerations, limitations, and opportunities. *Frontiers in genetics.* 2019;10:995.
4. Röttjers L, Faust K. From hairballs to hypotheses–biological insights from microbial networks. *FEMS microbiology reviews.* 2018;42(6):761–780.
5. Gloor GB, Macklaim JM, Pawlowsky-Glahn V, Egozcue JJ. Microbiome datasets are compositional: and this is not optional. *Frontiers in microbiology.* 2017;8:2224.
6. Kurtz ZD, Müller CL, Miraldi ER, Littman DR, Blaser MJ, Bonneau RA. Sparse and compositionally robust inference of microbial ecological networks. *PLoS computational biology.* 2015;11(5):e1004226.
7. Xiao Y, Angulo MT, Friedman J, Waldor MK, Weiss ST, Liu YY. Mapping the ecological networks of microbial communities. *Nature communications.* 2017;8(1):2042.
8. Kelliher JM, Johnson LY, Rodriguez FE, et al. A cost and community perspective on the barriers to microbiome data reuse. *Frontiers in Bioinformatics.* 2025;5:1585717.
9. Shetty SA, Kuipers B, Atashgahi S, Aalvink S, Smidt H, Vos dWM. Inter-species metabolic interactions in an in-vitro minimal human gut microbiome of core bacteria. *npj Biofilms and Microbiomes.* 2022;8(1):21.
10. Kodera SM, Das P, Gilbert JA, Lutz HL. Conceptual strategies for characterizing interactions in microbial communities. *IScience.* 2022;25(2).
11. Blöbaum P, Janzing D, Washio T, Shimizu S, Schölkopf B. Analysis of cause-effect inference by comparing regression errors. *PeerJ Computer Science.* 2019;5:e169. doi: 10.7717/peerj-cs.169
12. Culp EJ, Goodman AL. Cross-feeding in the gut microbiome: ecology and mechanisms. *Cell Host & Microbe.* 2023;31(4):485–499.
13. Borger MJ, Ramesh A. Let's DAG in: how directed acyclic graphs can help behavioural ecology be more transparent. *Proceedings B.* 2025;292(2051):20250963.
14. Srinivasan S, Jnana A, Murali TS. Modeling microbial community networks: methods and tools for studying microbial interactions. *Microbial ecology.* 2024;87(1):56.
15. Layeghifard M, Hwang DM, Guttman DS. Disentangling interactions in the microbiome: a network perspective. *Trends in microbiology.* 2017;25(3):217–228.
16. Faust K, Raes J. Microbial interactions: from networks to models. *Nature Reviews Microbiology.* 2012;10(8):538–550.
17. Ganter M, Kaltenbach HM, Stelling J. Predicting network functions with nested patterns. *Nature communications.* 2014;5(1):3006.
18. Lv X, Zhao K, Xue R, Liu Y, Xu J, Ma B. Strengthening insights in microbial ecological networks from theory to applications. *MSystems.* 2019;4(3):10–1128.
19. Jurburg SD, Blanco MJA, Chatzinotas A, et al. Datathons: fostering equitability in data reuse in ecology. *Trends in Microbiology.* 2024;32(5):415–418.
20. Krzywinski M, Birol I, Jones SJ, Marra MA. Hive plots—rational approach to visualizing networks. *Briefings in bioinformatics.* 2012;13(5):627–644.

SUPPORTING INFORMATION

Additional supporting information may be found in the online version of the article at the publisher's website.

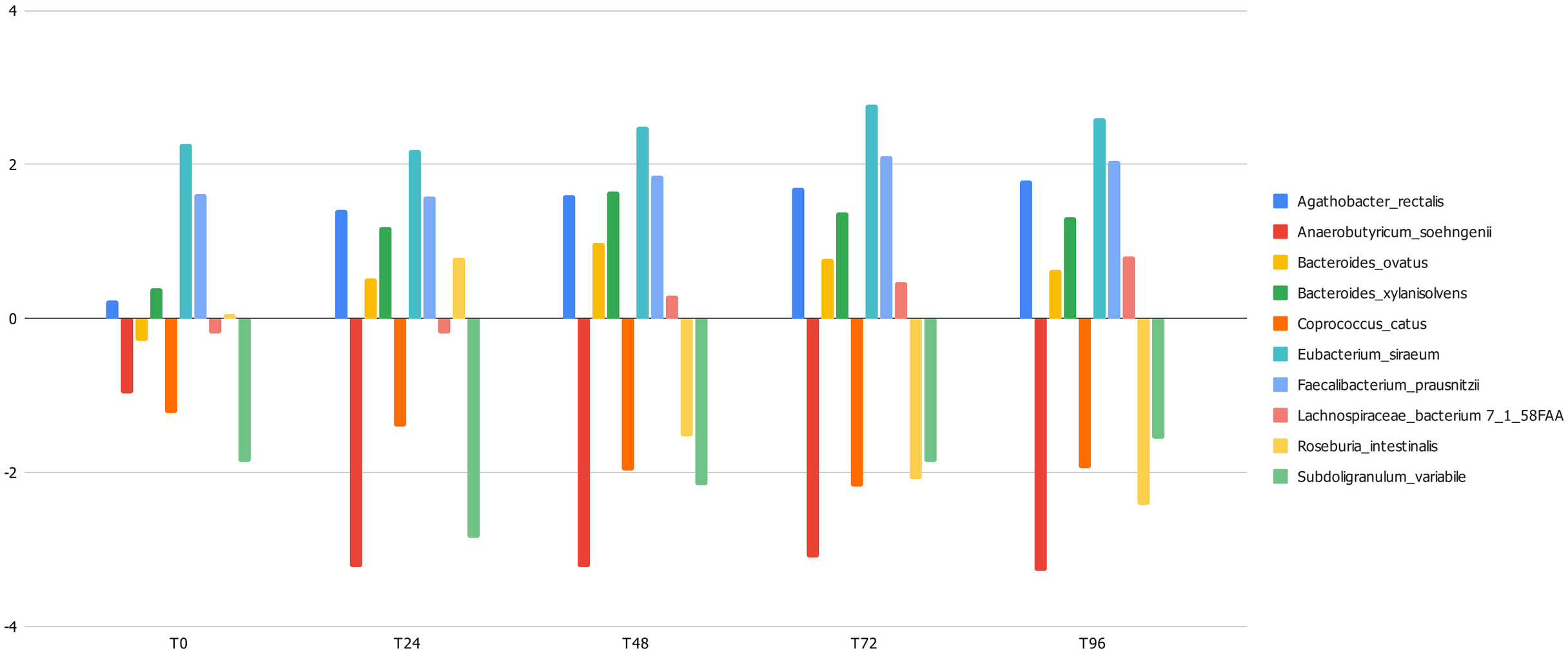
4
2
0
-2
-4
T0
T24
T48
T72
T96
Agathobacter_rectalis
Anaerobutyricum_soehngenii
Bacteroides_ovatus
Bacteroides_xylanisolvens
Coprococcus_catus
Eubacterium_siraeum
Faecalibacterium_prausnitzii
Lachnospiraceae_bacterium 7_1_58FAA
Roseburia_intestinalis
Subdoligranulum_variabile

A) T0

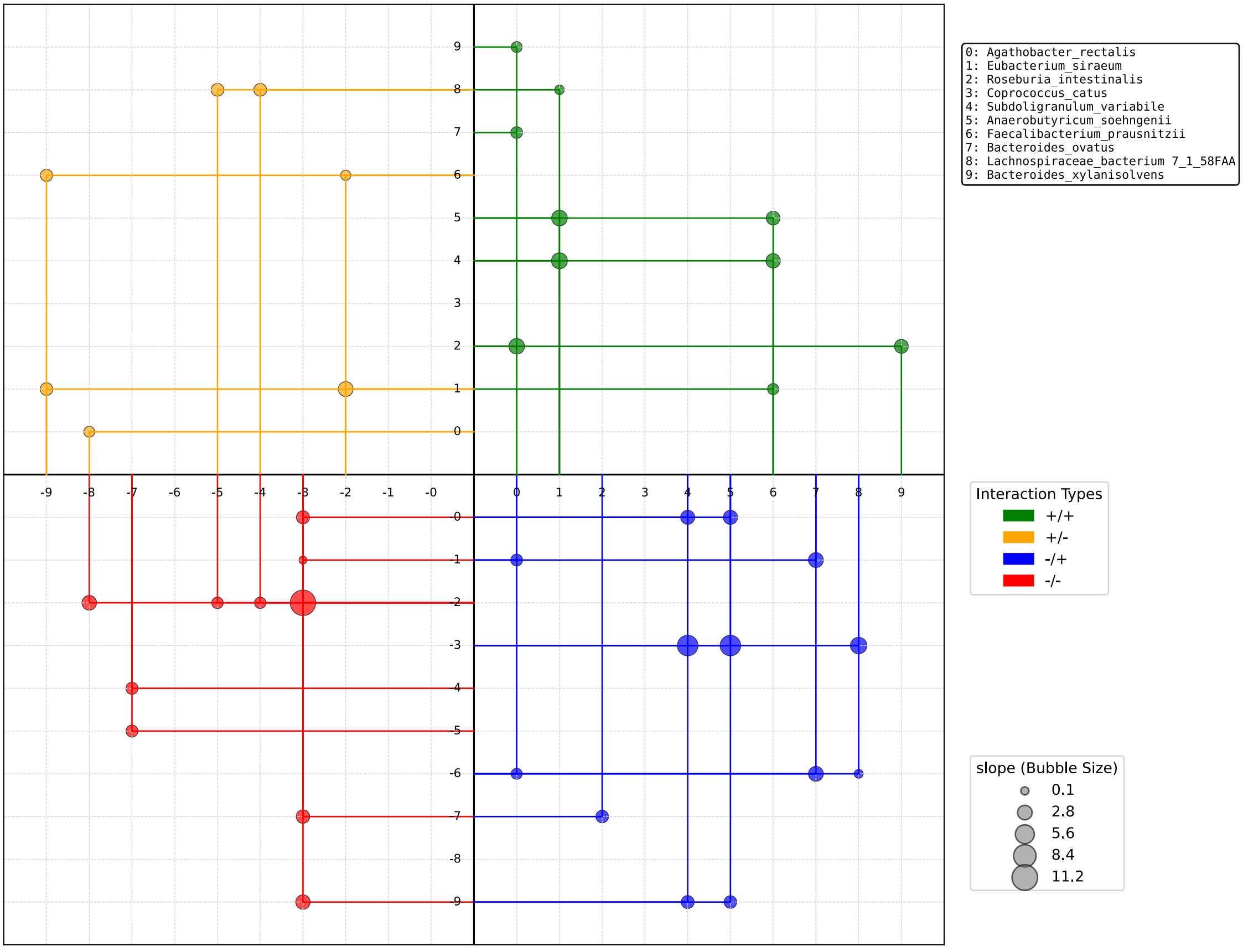
0: Agathobacter_rectalis
1: Eubacterium_siraeum
2: Roseburia_intestinalis
3: Coprococcus_catus
4: Subdoligranulum_variabile
5: Anaerobutyricum_soehngenii
6: Faecalibacterium_prausnitzii
7: Bacteroides_ovatus
8: Lachnospiraceae_bacterium 7_1_58FAA
9: Bacteroides_xylanisolvens
Interaction Types
+/+
+/-
-/+
-/-
slope (Bubble Size)
0.1
2.8
5.6
8.4
11.2

B) T24

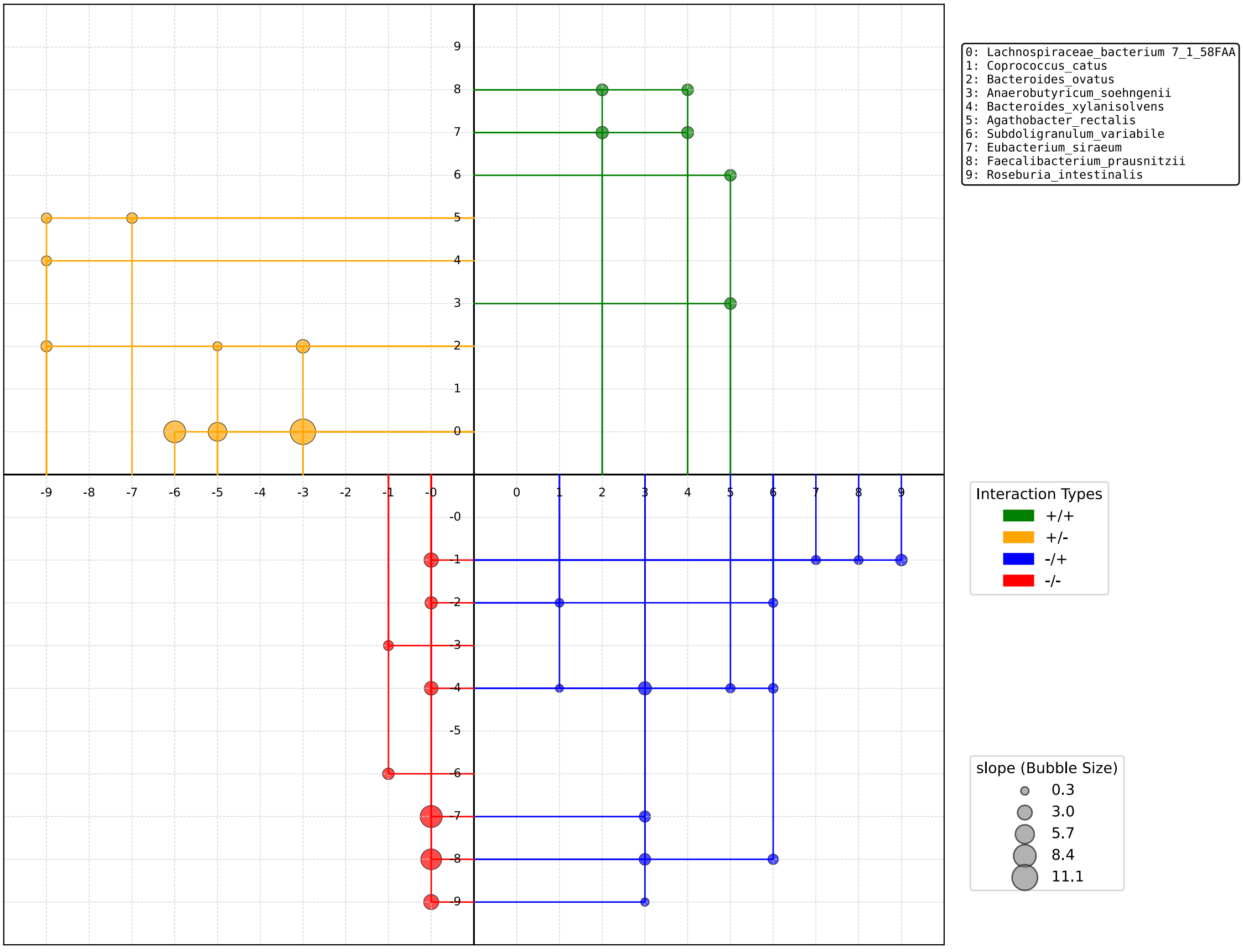
0: Lachnospiraceae_bacterium 7_1_58FAA
1: Coprococcus_catus
2: Bacteroides_ovatus
3: Anaerobutyricum_soehngenii
4: Bacteroides_xylanisolvens
5: Agathobacter_rectalis
6: Subdoligranulum_variabile
7: Eubacterium_siraeum
8: Faecalibacterium_prausnitzii
9: Roseburia_intestinalis
Interaction Types
+/+
+/-
-/+
-/-
slope (Bubble Size)
0.3
3.0
5.7
8.4
11.1

C) T48

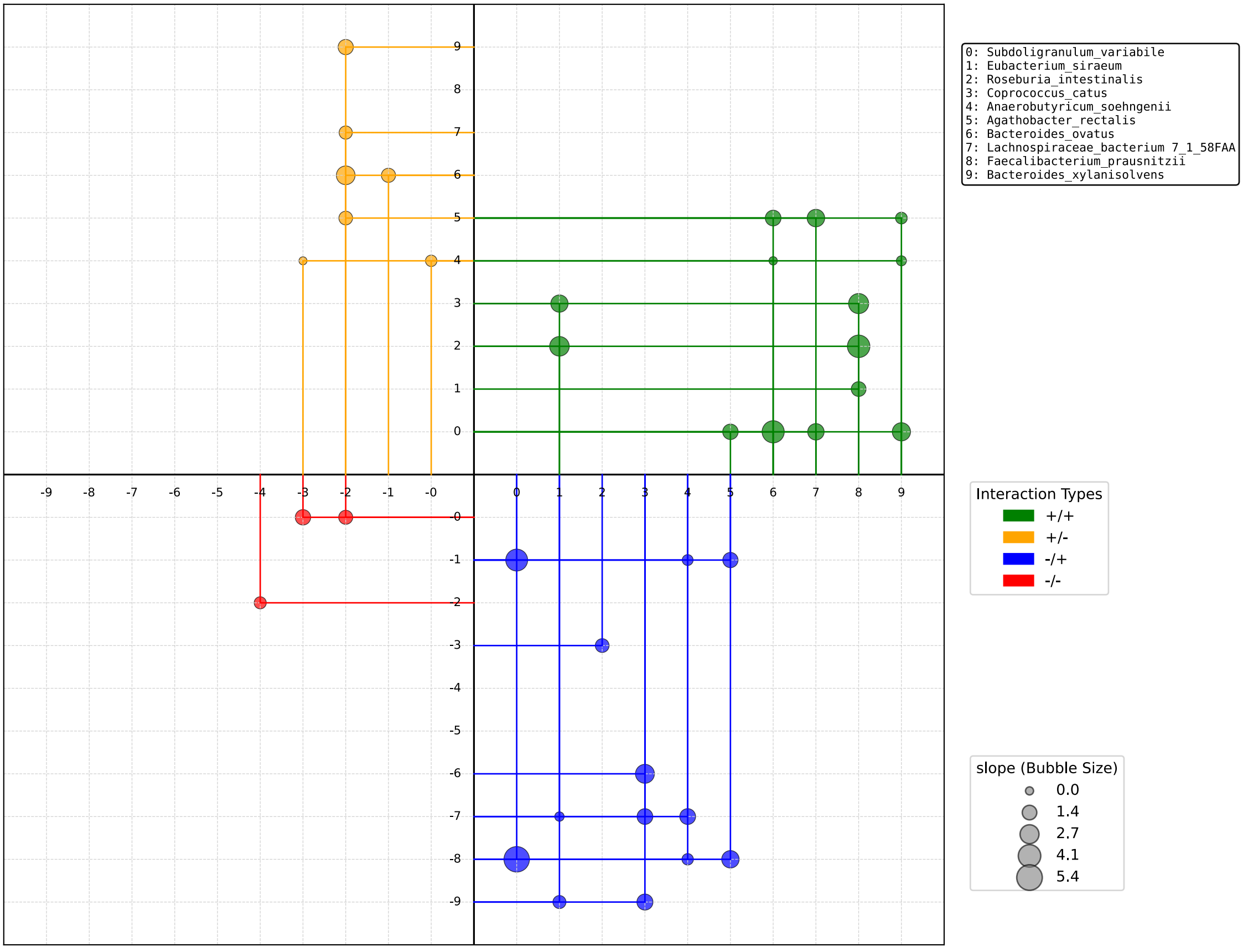
0: Subdoligranulum_variabile
1: Eubacterium_siraeum
2: Roseburia_intestinalis
3: Coprococcus_catus
4: Anaerobutyricum_soehngenii
5: Agathobacter_rectalis
6: Bacteroides_ovatus
7: Lachnospiraceae_bacterium 7_1_58FAA
8: Faecalibacterium_prausnitzii
9: Bacteroides_xylanisolvens
Interaction Types
+/+
+/-
-/+
-/-
slope (Bubble Size)
0.0
1.4
2.7
4.1
5.4

D) T72

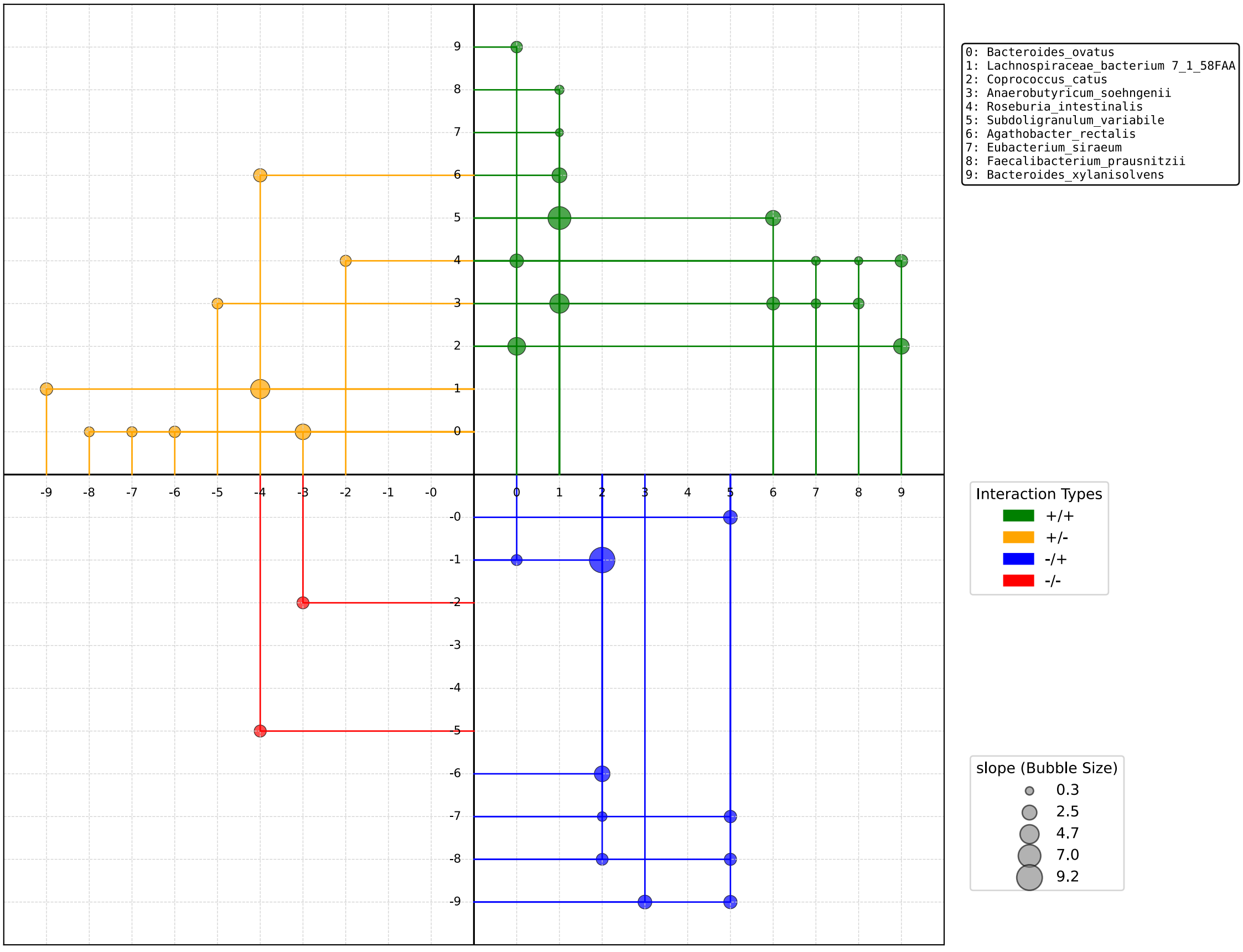
0: Bacteroides_ovatus
1: Lachnospiraceae_bacterium 7_1_58FAA
2: Coprococcus_catus
3: Anaerobutyricum_soehngenii
4: Roseburia_intestinalis
5: Subdoligranulum_variabile
6: Agathobacter_rectalis
7: Eubacterium_siraeum
8: Faecalibacterium_prausnitzii
9: Bacteroides_xylanisolvens
Interaction Types
+/+
+/-
-/+
-/-
slope (Bubble Size)
0.3
2.5
4.7
7.0
9.2

E) T96

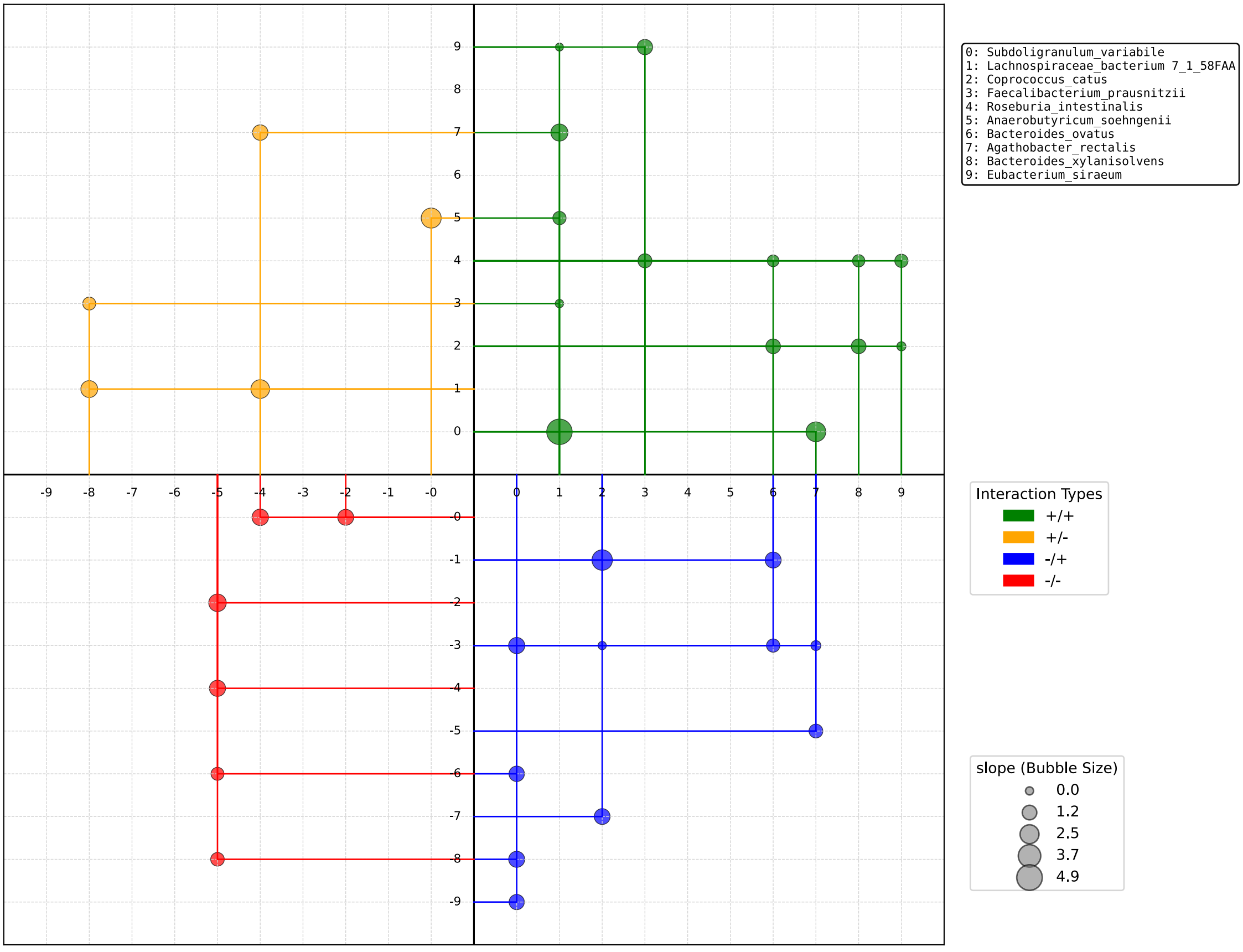
0: Subdoligranulum_variabile
1: Lachnospiraceae_bacterium 7_1_58FAA
2: Coprococcus_catus
3: Faecalibacterium_prausnitzii
4: Roseburia_intestinalis
5: Anaerobutyricum_soehngenii
6: Bacteroides_ovatus
7: Agathobacter_rectalis
8: Bacteroides_xylanisolvens
9: Eubacterium_siraeum
Interaction Types
+/+
+/-
-/+
-/-
slope (Bubble Size)
0.0
1.2
2.5
3.7
4.9